ELSEVIER

Polymer 42 (2001) 7313–7325

polymer

www.elsevier.nl/locate/polymer

Effect of viscosity ratio on structure evolution in miscible polymer blends

Heidi E. Burch[a], Chris E. Scott[b,*]

[a]Department of Chemical Engineering, Massachusetts Institute of Technology, Cambridge, MA 02139, USA
[b]Department of Materials Science and Engineering, Massachusetts Institute of Technology, Cambridge, MA 02139, USA

Received 7 February 2001; received in revised form 21 March 2001; accepted 23 March 2001

Abstract

Structure development through the softening/melting compounding regime is investigated for very-low-viscosity-ratio model miscible blends consisting of poly(styrene-co-acrylonitrile) (SAN)/poly(methyl methacrylate) (PMMA) and polyethylene (PE)/polyethylene. Blends with viscosity ratios of 1.12, 0.11, 0.03, 0.003, and 0.00015 are pigmented, compounded, and visually interrogated. These experiments reemphasize both the importance of the softening/melting regime to the development of morphology in low-viscosity-ratio, miscible blends, and the dynamic similarity between the behavior of these miscible blends and their immiscible counterparts at short mixing times. Additionally, these experiments reveal the presence of a phase-inversion-like process in the lowest viscosity-ratio blends, as evidenced by both local and global maxima in the mixer torque traces. This is the first such observation in a miscible polymer blend. We postulate a mechanism of morphology development that incorporates the Scott/Macosko lacing/sheeting mechanism, as well as the observed phase-inversion-like process. Finally, we confirm that the presence of a low-viscosity additive significantly delays the onset of mixing, even when thermodynamically miscible with the major component. © 2001 Elsevier Science Ltd. All rights reserved.

Keywords: Miscible polymer blend; Morphology development; Viscosity ratio

1. Introduction

The issue of mixing of low-viscosity, miscible additives into polymer matrices is of particular interest to the polymer processing community. A wide variety of commercial polymers are actually complex formulations that involve the incorporation of low-viscosity, miscible additives, including thermal stabilizers, processing aids, organic dyes, antioxidants, and plasticizers, into a high-viscosity polymer. Common examples include the compounding of plasticizers into poly(vinyl chloride) and cellulose esters, sometimes in concentrations approaching 50%, in order to convert these materials from stiff, hard materials into soft and rubbery ones.

While polymer–polymer mixing is never a trivial task because of the high viscosities and extremely low diffusivities of the materials involved, the problem is further exacerbated when one of the components has a significantly lower viscosity than the other(s). In polymer mixing operations it is crucial to achieve the desired level of mixing as rapidly as possible, with as little energy input as possible, in order to minimize thermal and shear degradation of the polymer matrix. However, the large mismatch between the additive's viscosity and that of the molten polymer greatly magnifies the difficulties associated with compounding these materials. This increased difficulty is due to the tendency of the low-viscosity component to segregate to the high shear rate regions in the mixing equipment, where it can actually retard mixing [1–3]. Clearly, there is a long-standing need for improved understanding of the mixing process in order to design more effective mixing equipment and to develop more efficient mixing protocols for the incorporation of low-viscosity miscible additives into polymers.

The problem of shear segregation is particularly insidious; in addition to the obvious obstacles to achieving a homogeneous mixture, this migration further hinders mixing because of its lubricative effects. While most experts agree that shear migration occurs because of the thermodynamic tendency to minimize the rate of viscous dissipation, and hence entropy production, [4,5] the phenomenon of shear migration also diminishes the rate of mixing. Tadmor and Gogos estimate that 80–90% of the energy used to transform solid polymer pellets to a molten fluid is generated by viscous dissipation [3]. Since viscous dissipation is directly proportional to viscosity and proportional to the shear rate squared, the presence of a low-viscosity fluid acting as a lubricant in the high-shear rate regions of the

* Corresponding author. Address: Exponent, 21, Strathmore Road, Natick, MA 01760, USA. Tel.: +1-508-652-8528; fax: +1-508-647-1899.
E-mail address: cscott@exponent.com (C.E. Scott).

0032-3861/01/$ - see front matter © 2001 Elsevier Science Ltd. All rights reserved.
PII: S0032-3861(01)00240-3

Table 1
Key physical properties of the SANs and PMMAs used in this study

Material	Grade	Melt flow index (g/10 min)	Viscosity at 180°C, 80 s^{-1} (Pa s)	Glass transition temperature (°C)
SAN	Tyril® 100	8.0 (at 230°C)	3.5×10^3	106
	MRY 5003c	–[a]	8.2×10^2	104
	MRY 5003e	–[a]	2.6×10^2	101
PMMA	VM	14.5 (at 190°C)	3.9×10^3	92
	V825	3.7 (at 190°C)	7.6×10^3	109

[a] Not determined for this material.

equipment, where viscous dissipation should be maximized, dramatically decreases the energy available to transform the high-viscosity, major phase material from a solid to a fluid, and hence, decreases the rate of mixing.

The academic community has largely overlooked the problem of mixing low-viscosity, miscible additives into polymeric matrices, along with the associated issues of additive migration and its effects on the evolution of structure in the resulting blend. Mixing and morphology development in immiscible polymer blends of similar viscosity have been addressed by a variety of researchers [6–8], but similarly extensive treatments of miscible mixing are lacking. There are several theoretical works that deal with mixing in miscible systems [2,9–12], but these works have dealt almost exclusively with mixing in the fluid state. There have been a few experimental investigations into miscible blends [13–15], but these are by no means comprehensive or conclusive and they have likewise largely subverted the softening/melting regime, shown to be of particular importance to morphological evolution in immiscible blends by several researchers [6,8,16]. Recent efforts in our laboratory have endeavored to correct this deficit [17] by examining the evolution of structure in miscible blends with viscosity ratios near one through real softening/melting regime processes. The goal of this work is to extend our understanding of miscible polymer mixing by performing the first systematic study of low-viscosity-ratio, miscible blends compounded through the softening/melting regime and the effects of the viscosity ratio of such a system upon its morphology.

2. Experimental

Two model miscible blends were chosen for this work. The first was composed of poly(methyl methacrylate) (PMMA) and poly(styrene-co-acrylonitrile) (SAN), while the other consisted of two miscible polyethylenes (PE).

2.1. PMMA/SAN blend materials characterization

The PMMAs used in the first series of blends were AtoHaas Plexiglas® VM and V825 resins, while the SANs were Dow Tyril® 100 and two custom-synthesized SANs from Bayer Corporation. Traditionally, mixing in miscible systems has been studied using the same fluid for both phases, then differentiating them by pigmentation. However, previous work in this laboratory [17] utilized a PMMA/SAN blend, which also provided for mixture characterization using infrared spectroscopy, so it was chosen for comparison purposes.

In a limited range of acrylonitrile content, typically cited as 10–30 wt%, SAN is completely miscible with PMMA across the composition range [18]. The acrylonitrile content of all the SANs was approximately 25 wt%; in the case of the Tyril® 100 SAN, this was verified by elemental analysis, and in the case of the custom-synthesized material, the SAN content was known a priori. Differential scanning calorimetry (DSC) was used to determine the glass transition temperature of each of these amorphous polymers. Results are given in Table 1, along with other key properties.

2.2. PE/PE blend materials characterization

The PEs selected for the second series of blends were Epolene® waxes available from Eastman Chemical Company. Specifically, Epolene® C-14 was blended with either Epolene® C-15 or Epolene® N-11, all of which are low-density PEs. The miscibility of polyethylene blends is not guaranteed a priori; however, Hu and co-workers, as well as Norton and Keller [19,20] maintain that the presence of a single melting endotherm in DSC is indicative of cocrystallization in polyethylene blends. Furthermore, cocrystallization of PEs is considered a powerful indicator of melt miscibility [21,22]. DSC was performed on all the pure C-14, C-15, and N-11, as well as 50 wt%/50 wt% blends of the C-14 with the C-15 and the N-11. Based on the appearance of a single melting endotherm for both the C-14/C-15 and C-14/N-11 blends in these experiments, it can be concluded that these blends are indeed melt-miscible. Key material properties are given in Table 2.

2.3. Rheological characterization

The SANs, PMMAs, and C-14 PE were rheologically characterized in a Rheometrics ARES mechanical spectrometer operating in the parallel-plate dynamic strain mode. Measurements were taken at small enough strains,

Table 2
Key physical properties of the Epolene® polyethylenes used in this study

Grade	Ring and ball softening point (°C)	Molecular weight, M_w	Molecular weight, M_n	Melt index (g/10 min at 190°C)	Viscosity at 180°C, 80 s^{-1} (Pa s)
C-14	> 133	143,000	18,000	1.6	7.6×10^2
C-15	102	17,000	6700	4200	2.1[b]
N-11	108	6000	2000	–[a]	0.02[b]

[a] Not determined for this material.
[b] Determined in steady-shear at 100 s^{-1}.

depending on the material, to insure that the material's response was in the linear viscoelastic regime. Viscosities at 180°C and 80 s^{-1} were chosen as representative of the actual conditions experienced by the material during drag flow in melt compounding. Dynamic strain experiments revealed the C-15 and N-11 PEs to be Newtonian at 180°C, so their viscosities were determined in steady shear at a shear rate of 100 s^{-1}. Based on these experiments, viscosity ratios, defined as $\lambda = \eta_{minor}/\eta_{major}$, of 1.12, 0.11, and 0.03 were obtained using the SAN/PMMA blends, while the PEs blends had viscosity ratios of 0.003, and 0.00015. Key material properties are given in Table 2, and specific blend compositions as a function of viscosity ratio are given in Table 3.

For all of the experiments discussed here, the blend composition is 90 wt% major component/10 wt% minor component. This composition is representative of additive concentrations used in commercial formulations. Furthermore, in some cases the feed material was mixed, with the major component in pellet form, and the minor component in powder form. Details of this are given in Table 3. This is characteristic of industrial compounding formulations, which typically incorporate powdered additives, such as antioxidants and pigments. The physical form of the constituents is known to influence processing behavior [23]. The powder feeds were prepared by grinding either pigmented chunks (VM PMMA), as-received pellets (VM PMMA), or as-received flake (MRY 5003c and MRY 5003e SAN) in a water-cooled IKA Universalmühle M20 ceramic powder mill. The VM PMMA powders was prepared by grinding 50 g batches of pellets/chunks for 5 min each, while the MRY SAN powders were prepared by grinding 50 g batches for 30 s. Due to the inherently smaller initial particle size of the SANs, the resulting powders had approximately the same particle size.

2.4. Preparation of pigmented materials

Pigmentation of one or both blend components was used to provide contrast for visual analysis of the mixing process. Details of the contrast scheme as a function of viscosity ratio are given in Table 3. The pigmented major-component materials used were prepared by dilutions of masterbatches. The Tyril® 100 SAN, V825 PMMA, and C-14 PE were pigmented at 0.1 wt% titanium dioxide with DuPont R103 TiO_2 by first compounding the TiO_2 into the respective resins at 1.0 wt% using the batch intensive mixer. The mixtures were thoroughly compounded at 50 rpm before being pressed into 3.18 mm thick plaques, which were then cut into 3 mm cubes with either a saw (SAN, PMMA) or scissors (PE). Then, the masterbatch pellets were premixed in buckets with sufficient virgin resin to dilute the pigment to 0.1 wt%, before being compounded in the single-screw extruder and repelletized.

The minor-phase VM PMMA was pigmented at 0.1 wt% carbon black by compounding N339 carbon black into VM PMMA at that concentration using the batch intensive mixer. The mixture was thoroughly compounded at 50 rpm before being pressed into a 3.18 mm thick plaque, which was then cut into $6 \times 6 \times 3$ mm chunks with a saw. These chunks were then ground into powder using the Universalmühle M20 ceramic powder mill.

The pigmentation of the C-15 and N-11 PEs was accomplished using a dispersion of carbon black in a liquid hydrocarbon matrix, in this case ColorFlo's CK-1201. Due to the exceptionally low melt viscosities of these two PEs, these

Table 3
Blend compositions and contrasts as a function of viscosity ratio

Viscosity ratio	Major component	Minor component	Contrast mechanism (Major/Minor)
1.12	Tyril® 100 SAN Pellets	VM PMMA Powder	White/Black
0.11	V825 PMMA Pellets	MRY 5003c SAN Powder	White/Clear
0.03	V825 PMMA Pellets	MRY 5003e SAN Powder	White/Clear
0.003	Epolene® C-14 PE Pellets	Epolene® C-15 PE Pellets	White/Black
0.00015	Epolene® C-14 PE Pellets	Epolene® N-11 PE Pellets	White/Black

materials were melted separately in beakers submersed in a temperature-controlled silicone oil bath, rather than in a batch mixer. Then, the carbon black dispersion was added to each at a concentration of 1 wt% with external stirring. After the mixtures were thoroughly blended, they were poured into heated 3.18 mm thick picture-frame molds and maintained at temperature for 5 min to remove any entrained air bubbles. The molds were cooled to room temperature, then the materials were cut into approximately 3 mm cubes using a papercutter and scissors.

These pigment concentrations were chosen because they afforded the best compromise between color saturation and lack of rheological impact. Additionally, the contrast mechanisms (white/black, white/clear) were chosen to provide the optimum visual contrast without losing precious amounts of the custom-synthesized MRY SANs to extruder hold-up during repelletization.

2.5. Blend preparation

All the compounding runs were performed in a Haake Rheomix 600 batch intensive mixer utilizing roller blades at 50 rpm. Batch masses were calculated based on material densities to give a constant batch size of approximately 50 cm^3, corresponding to a 72% degree of fill. The PMMAs and SANs were dried overnight at 60°C under vacuum before processing, while the PEs, which are significantly less hygroscopic, were used as is. Prior to compounding, the feed materials were mixed in the chosen 90 wt% major phase/10 wt% minor phase proportions in a cup. For the SAN/PMMA blends (those with viscosity ratios of 1.12, 0.11, and 0.03), the feed material consisted of pellets of the major phase and powdered minor phase, while for the PE/PE blends (those with viscosity ratios of 0.003 and 0.00015), the feed materials were both pellets; however, a pellet/pellet blend with a viscosity ratio of 1.12 was also prepared for comparison purposes. The salt-and-pepper mix was then added to the mixer, which had been preheated to 180°C, and was compounded for the desired length of time. For $\lambda = 1.12$, samples were prepared at 30, 45, 60, 90 s, 2, 3 and 4 min mixing, at which time the blend appeared homogeneous to the naked eye. For $\lambda = 0.11$, samples were prepared at 30, 45, 60 and 90 s mixing in an effort to ascertain the early stages of morphological evolution in a median-range viscosity-ratio blend. For $\lambda = 0.003$ and $\lambda = 0.00015$, sample times were chosen based on the torque profile of long-mixing time runs, which will be discussed in more detail later. However, for $\lambda = 0.003$, samples were prepared at 16, 24, 32, 46, 60 s, and 5 min mixing time. For the $\lambda = 0.00015$ blend, samples were prepared at 20, 30, 36, 60, 80 s, and 5 min mixing time. At the cessation of mixing, depending on the state of the molten blend, it was either quenched in liquid nitrogen or pressed to 3.18 mm thick in a picture-frame mold between 180°C platens for 30 s before being cooled in situ to room temperature using cooling water (~10 min). The influence of diffusion during pressing should be virtually nonexistent, as the diffusivity of the SAN/PMMA blend is on the order of 10^{-14} cm^2/s at 180°C [24] and that of the PE/PE blend ranges from 5×10^{-8} to 1×10^{-10} cm^2/s at 175°C, depending on the molecular weights of the materials involved [25].

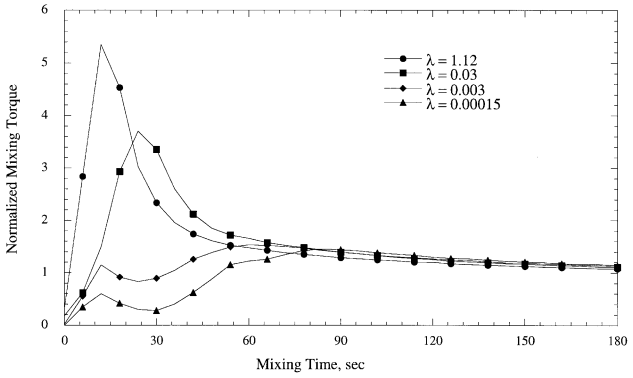

Fig. 1. Normalized Haake batch intensive mixer torque traces for $\lambda = 1.12$, $\lambda = 0.03$, $\lambda = 0.003$, and $\lambda = 0.00015$ blends. The torque is normalized by the steady-state mixing torque for each viscosity.

Optical microscopy was performed on pigmented samples that were cut from a larger sample plaque, embedded in epoxy, and polished using a rotary polisher. The final level of polishing was 0.05 μm alumina powder. The polishing regimen provided an excellent flat surface with minimal scratches on which to conduct optical microscopy investigations. A Zeiss microscope equipped with a 35 mm camera was used to capture the micrographs. Additional micrographs were obtained on a Zeiss microscope equipped with a digital camera and screen-capture software.

3. Results

3.1. Mixing torque traces

Mixing torque traces from the Haake batch intensive mixer are shown in Fig. 1 for the $\lambda = 1.12$, $\lambda = 0.03$, $\lambda = 0.003$, and $\lambda = 0.00015$ polymer blends. Due to the differences in absolute viscosity, which directly affect the mixing torques, the mixing torques were normalized by their respective long-time mixing torques. The $\lambda = 0.11$ curve, which is largely concurrent with the $\lambda = 0.03$ curve, has been omitted in the interest of brevity.

This figure clearly shows an inverse relationship between the viscosity ratio and the time required to achieve the maximum mixing torque. Specifically, in the $\lambda = 1.12$ blend, the maximum torque peak is achieved at 12 s mixing time, while for the $\lambda = 0.00015$ blend, the maximum torque is not reached until 84 s mixing. Additionally, the torque traces for the $\lambda = 0.003$ and $\lambda = 0.00015$ blends show both a local and a global maximum.

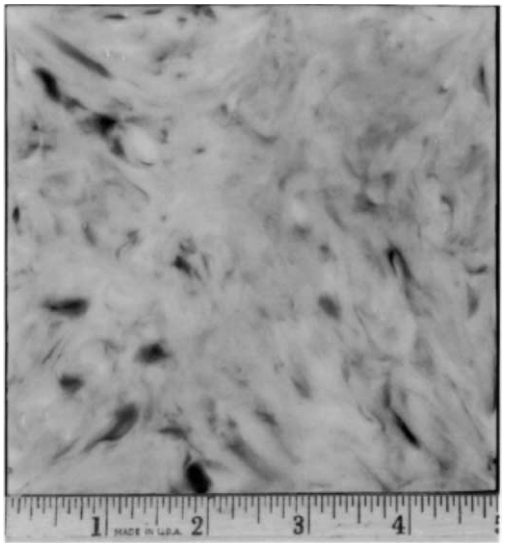

Fig. 2. Low magnification photographs of $\lambda = 1.12$ miscible polymer blends composed of 90% white SAN pellets/10% black PMMA pellets at 30 s mixing time.

3.2. Photographic observations

Representative low-magnification photographs of these low-viscosity ratio, miscible polymer blends are shown in Figs. 2–5. For the $\lambda = 1.12$ blend, only the 30 s mixing time sample is shown, while for $\lambda = 0.03$ blends, the 30 and 45 s mixing time samples are shown. Longer time samples for these blends appear homogeneous at this magnification. This is not the case, however, for the $\lambda = 0.003$ and $\lambda = 0.00015$ blends, so they are shown over a longer mixing time. These photographs clearly reveal that at a given mixing time the amount of undeformed major-phase pellets increases as the viscosity ratio decreases. They also demonstrate that undeformed pellets persist to longer times as the viscosity ratio decreases.

The photographs of the $\lambda = 0.003$ and $\lambda = 0.00015$ blends, shown in Figs. 4 and 5, are of particular interest.

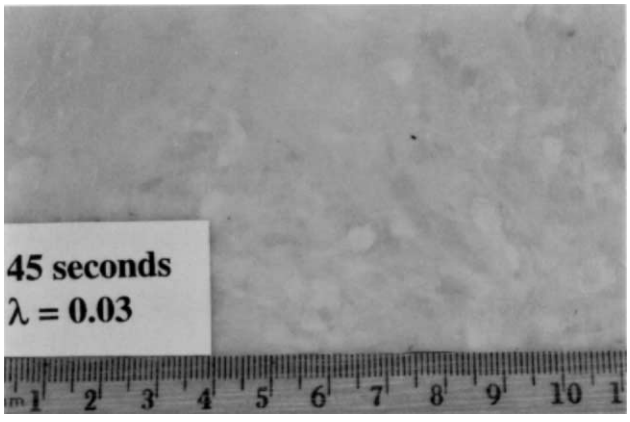

Fig. 3. Low magnification photographs of $\lambda = 0.03$ miscible polymer blend composed of 90 wt% white PMMA pellets and 10 wt% clear SAN powder at 45 s mixing time.

These photographs reveal two remarkable facts about the evolution of morphology in very-low-viscosity-ratio miscible blends. First and foremost, Fig. 4(a) shows that the initial morphology consists of largely-undeformed (white) major-phase pellets embedded in or encapsulated by a continuous matrix of molten (black) minor-phase material. These two early-time samples were not pressed into flat squares because that operation would have destroyed this granular texture. Second, as Fig. 4(b) and (c) demonstrate, the transition from this early, granular, dispersed-major-phase-pellet morphology to one that is largely molten and amalgamated happens very quickly. In the case of the $\lambda = 0.003$ blend shown here, at 46 s mixing time the blend morphology is dispersed pellets; by 60 s mixing time, the blend is consolidated into a melt, necessitating that it be pressed into a square sample. For the $\lambda = 0.00015$ blend, this same transition occurs between 36 and 60 s mixing time, although to a slightly lesser extent, as a comparison of Figs. 4(c) and 5(a) reveal. By 5 min mixing time, the blend is fully homogeneous, as shown in Fig. 5(c).

3.3. Microscopic observations

Representative and illustrative optical micrographs of the $\lambda = 1.12$, 0.11, and 0.03 blends at 30 s mixing time, as well as the $\lambda = 0.003$ blend at 16 s mixing time and the $\lambda = 0.00015$ blend at 60 s mixing time, are shown in Figs. 6–10. Figs. 6, 7(a), (b), and 8(b) show sheets of material in which holes are nucleating, as well as small droplets of material that have been formed. Figs. 7(b) and (c), as well as Fig. 8(a), illustrate the dichotomy of characteristic size scales present in these blends at short mixing times, with largely undeformed pellet cores of approximately 3 mm in size coexisting alongside droplets 100 μm or less in diameter. Furthermore, Fig. 7(a) depicts the rather-extensive interstitial morphology that is seen in these low-viscosity-ratio blends. The amount of this interstitial morphology increases as mixing time increases. Fig. 9 depicts two largely-undeformed major-phase pellets dispersed in a matrix of molten, minor-phase material, while Fig. 10 shows that, for extremely low-viscosity-ratio blends, by 60 s mixing time, there are very few resolvable morphological features. This may be due to either the limit of size resolution of optical microscopy or the limit of resolution of the contrast scheme. That is, at 60 s mixing time, the features may be too small to be seen with an optical microscope, or the pigment particles may be so well-dispersed that individual morphologies, while large enough to be seen, cannot be resolved due to lack of contrast.

4. Discussion

Previous research in this laboratory [17] has demonstrated the remarkable short-time similarities between the morphological development of immiscible polymer blends

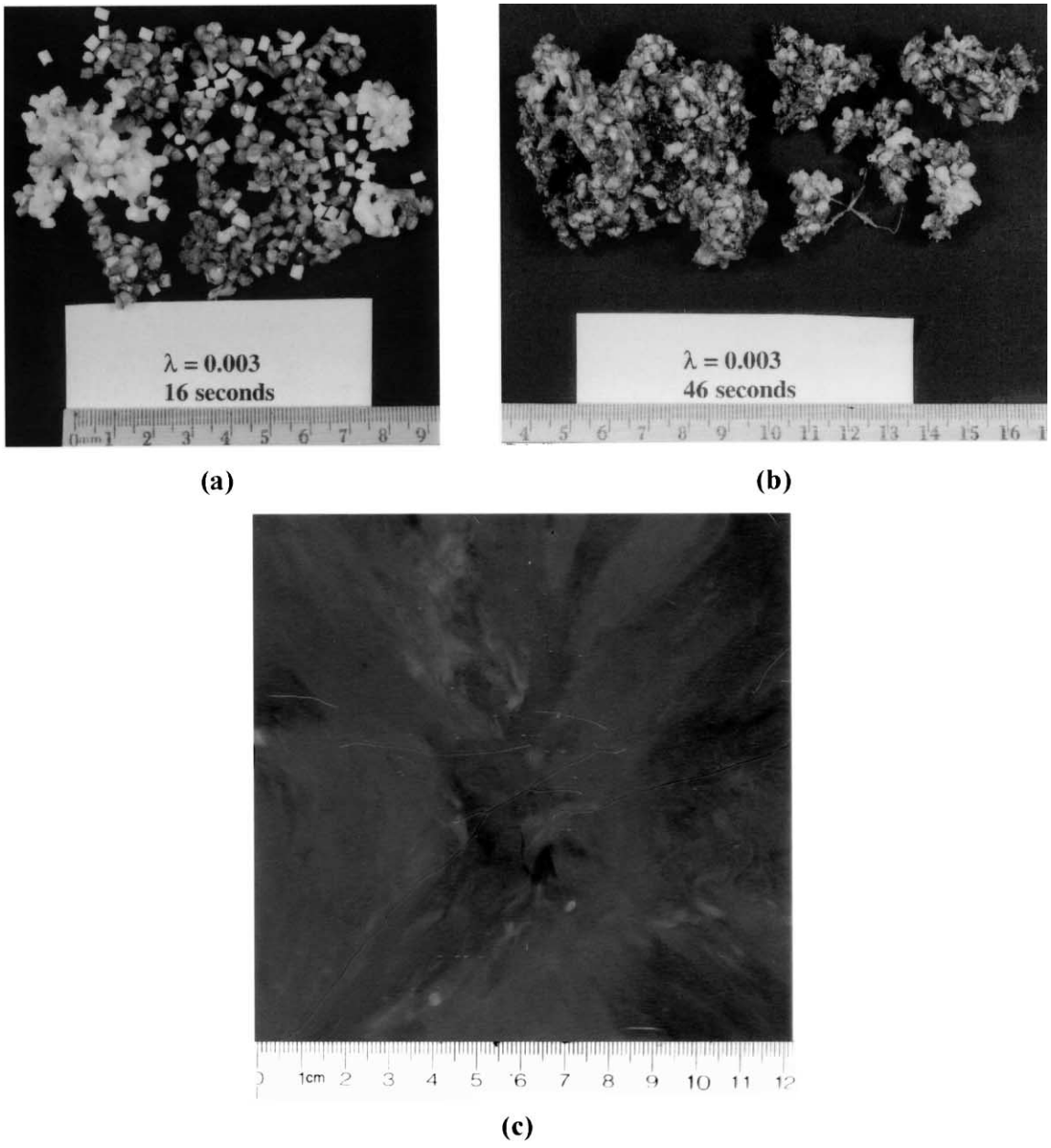

Fig. 4. Low magnification photographs of $\lambda = 0.003$ miscible polymer blend composed of 90 wt% white C-14 PE pellets and 10 wt% black C-15 pellets. (a) 16 s mixing time. (b) 46 s mixing time. (c) 60 s mixing time.

and that of miscible polymer blends for viscosity ratios of approximately one, namely the importance of the softening/melting regime to the development of the morphological features, and the operation of the Scott/Macosko lacing/sheeting mechanism, which rapidly generates a dichotomy of characteristic size scales. Previous investigations into low-viscosity ratio immiscible blends [23,26], have shown the paramount importance of the softening/melting regime in determining the morphology of these immiscible blends. Current work, which extends these investigations to very-low-viscosity-ratio miscible polymer blends reveals that this similarity persists to even very low viscosity ratios.

The continued importance of the softening/melting regime to the morphological development is the first key similarity between miscible and immiscible low-viscosity-ratio polymer blends. At 30 s mixing time, at which the micrographs shown in Figs. 6–8 were taken, these blends are well within the softening/melting regime of the compounding operation. This can be confirmed by previous work in the case of the $\lambda = 1.12$ blend, [17], and by Fig. 1 for the other blends, which shows that at 30 s mixing time, the torque has not begun to approach the steady-state values characteristic of the fluid–fluid mixing regime, where viscosities and hence, torques, are relatively constant. These micrographs demonstrate the dramatic decrease in the characteristic morphological size scale that occurs in

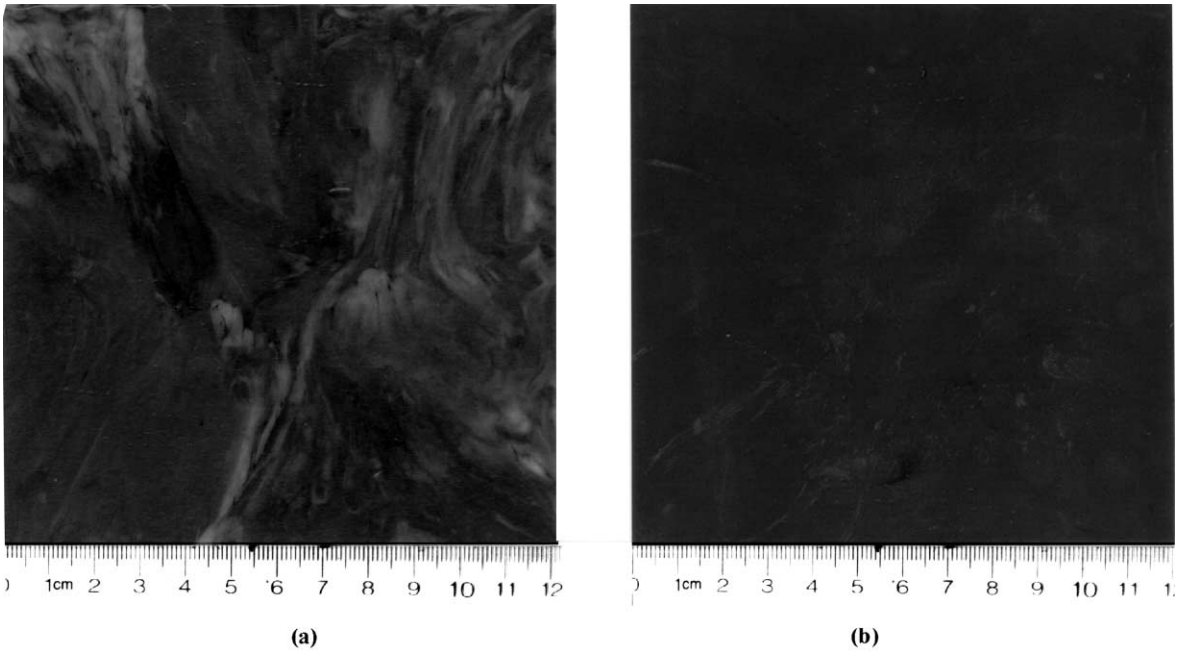

Fig. 5. Low magnification photographs of $\lambda = 0.00015$ miscible polymer blend composed of 90 wt% white C-14 PE pellets and 10 wt% black N-11 pellets. (a) 60 s mixing time. (b) 5 min mixing time.

the softening/melting regime. Figs. 7(a), (b) and 8(a), in particular, show the dichotomous nature of size scales that arises due to the softening/melting regime. These micrographs show largely-undeformed pellet cores of approximately 3 mm coexisting alongside droplets, holes, and striations with characteristic size scales of 50 μm or less. This reconfirms the previous work, which demonstrated the importance of the softening/melting regime for $\lambda \approx 1$ miscible blends, and extends the known importance of this regime to viscosity ratios on the order of 10^{-4} (micrographs of these blends showed principally the same features but were omitted in the interest of brevity). This further strengthens the conclusion that a dynamic similarity exists between miscible and immiscible blends at short mixing times.

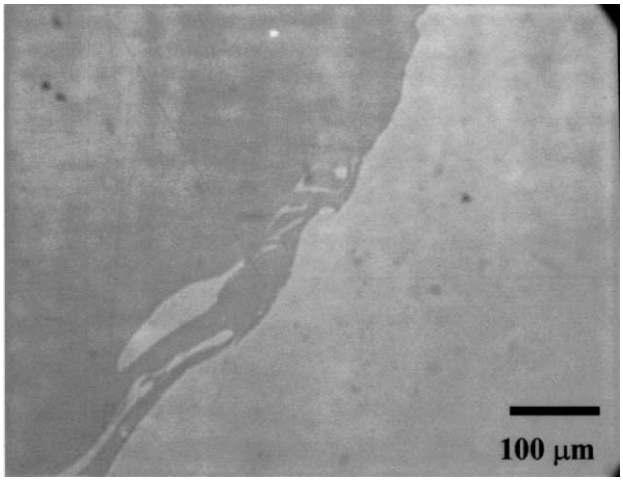

Fig. 6. Optical micrograph of a polished region of the $\lambda = 1.12$, 30 s mixing time blend composed of 90% white SAN pellets/10% black PMMA powder. Note the presence of the holes in the sheet of material.

Another observation that re-emphasizes both the importance of the softening/melting regime and the dynamic similarity between miscible and immiscible blends is the operation of the Scott/Macosko lacing/sheeting mechanism in these low-viscosity-ratio miscible blends. Previously thought to be active only in immiscible blends due to its reliance upon interfacial tension [6,16], previous work with miscible blends has shown that this mechanism does indeed operate in miscible blends, at least for viscosity ratios of approximately one [17]. However, Figs. 6, 7, 8(a) and (b) show morphologies of largely-undeformed pellets coexisting with large sheets of material in which holes are nucleating, as well as with very small-scale droplets. These are the hallmark morphologies of the mechanism, confirming its operation in blends with viscosity ratios as small as 10^{-4}. It is interesting to note that this morphological mechanism is largely unaffected by the use of the powdered SAN as the minor-phase component in the $\lambda = 1.12$, 0.11, and 0.03 blends. It appears that as long as the major phase is in pellet form, the Scott/Macosko mechanism will be operational.

Another significant observation that reinforces this idea of dynamic similarity between miscible and immiscible blends at short mixing times is that of an apparent phase inversion behavior in the $\lambda = 0.003$ and $\lambda = 0.00015$ PE blends. The normalized mixing torque traces for these two blends, shown in Fig. 1, exhibit both a local and global maximum. This is reminiscent of the torque traces seen during the compounding of low-viscosity-ratio, phase-inverting immiscible polymer blends [23,27,28]. In immiscible

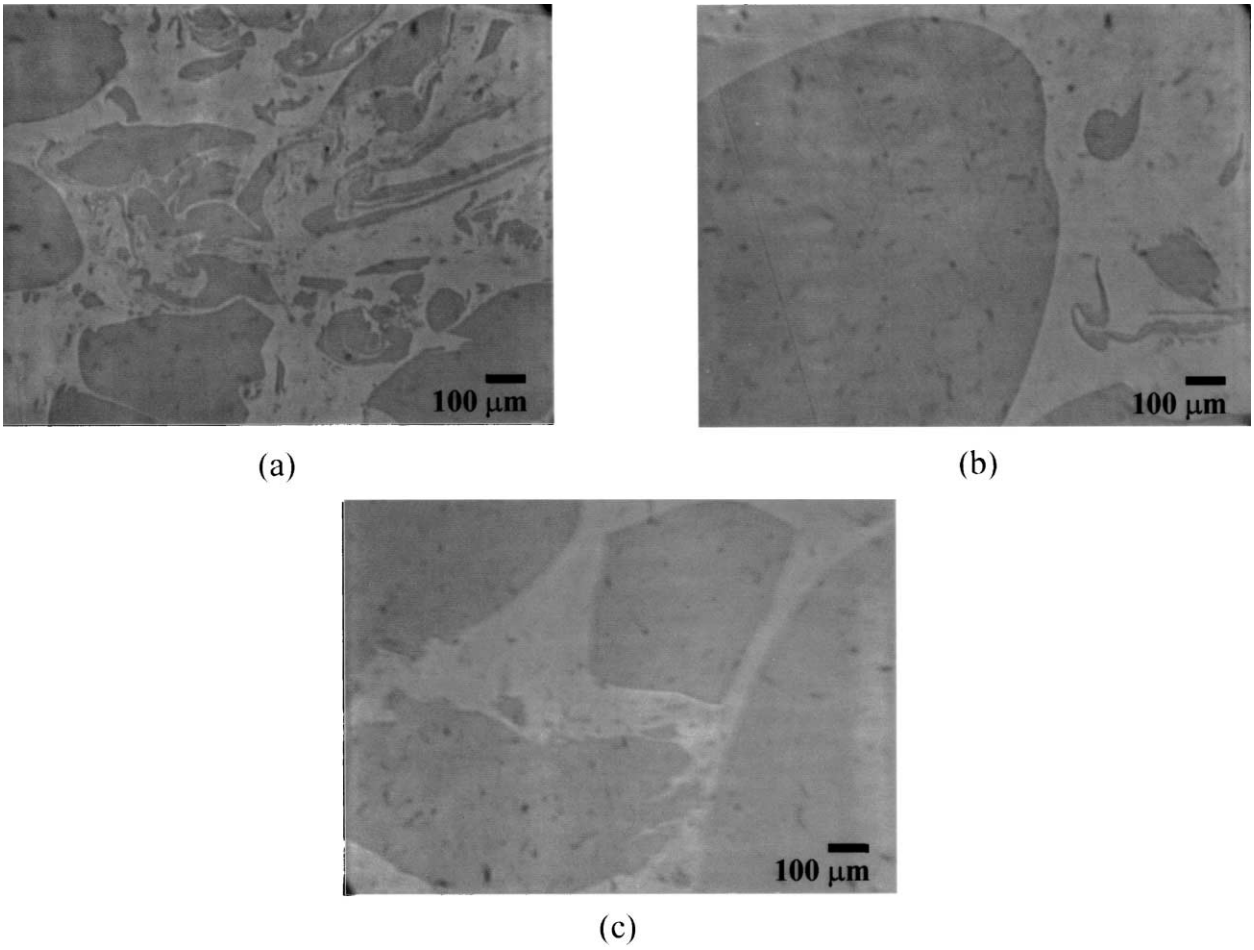

Fig. 7. Optical micrographs of polished regions of the $\lambda = 0.11$, 30 s mixing time blend composed of 90% white PMMA pellets/10% clear SAN powder.

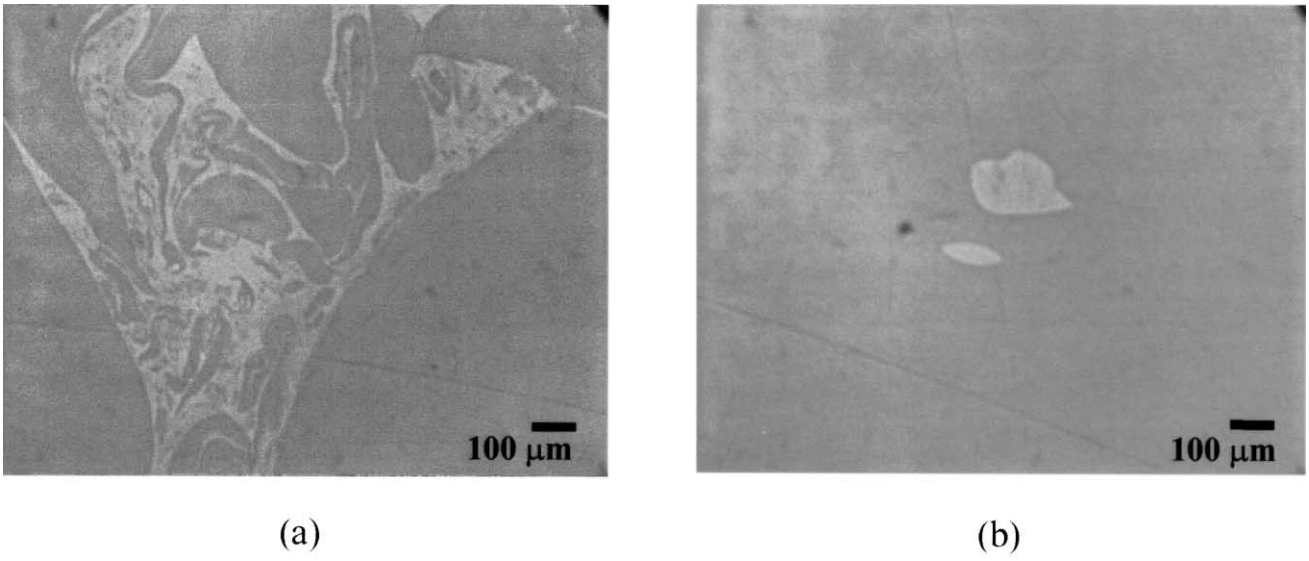

Fig. 8. Optical micrographs of polished regions of the $\lambda = 0.03$, 30 s mixing time blend composed of 90% white PMMA pellets/10% clear SAN powder.

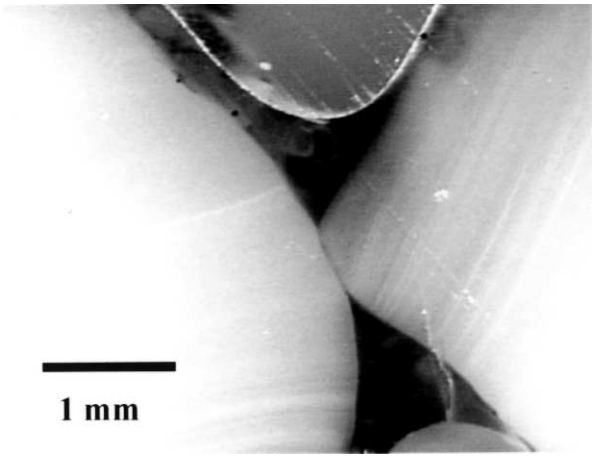

Fig. 9. Optical micrograph of a polished region of the $\lambda = 0.003$, 16 s mixing time blend composed of 90% white C-14 PE pellets/10% black C-15 PE pellets.

blends, the small torque peak is associated with the feeding stage, while the larger, global maximum in torque has been shown to correspond to the melting and attendant phase inversion that results in the more-viscous major component becoming the continuous phase. Visual confirmation of this phase inversion-like behavior is found in the early-mixing-time photographs and micrographs shown in Figs. 4 and 9. These pictures show a morphology of solid, major-phase pellets dispersed in a matrix of molten minor-phase material at short mixing times, followed by a largely-molten, consolidated morphology at approximately 60 s mixing time. These observations are consistent with the observation of both a local and a global maximum in the torque trace, reminiscent of phase inversion in immiscible blends. In phase-inverting immiscible blends, the low-viscosity minor component melts readily and initially becomes the continuous phase, corresponding to the first local torque peak. This low-viscosity component acts as a lubricant

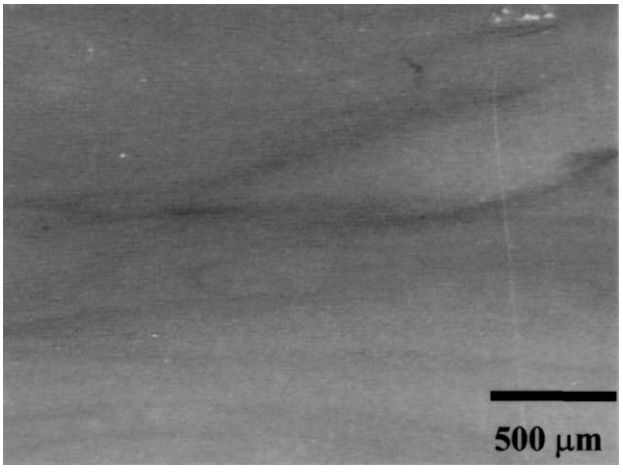

Fig. 10. Optical micrograph of a polish region of the $\lambda = 0.00015$, 60 s mixing time blend composed of 90% white C-14 PE pellets/10% black N-11 PE pellets.

and delays the softening of the major-phase pellets for some time, until they eventually melt and coalesce, resulting in the second, global torque peak [23]. In the case of these miscible blends, the timing of the appearance of the molten, consolidated morphology corresponds quite well to the timing of the maximum torque peaks shown in Fig. 1.

It is important to note that these observations constitute only a phase-inversion-like behavior, not a true phase inversion, because in miscible blends, the final morphology is a single-phase system, rather than droplets of the minor phase dispersed in a major-phase matrix, as in immiscible polymer blends. Additionally, this phase-inversion-like behavior in miscible blends differs slightly from that seen in immiscible blends in its initial onset viscosity ratio. Previous workers in this laboratory have observed phase inversion in immiscible polymer blends beginning around viscosity ratios of 0.3, while onset for these miscible blends is not seen until $\lambda = 0.003$, a difference of two orders of magnitude [23,26]. This is most likely due to the fact that this phase-inversion-like process occurs so rapidly in the $\lambda = 0.11$ and $\lambda = 0.03$ that it cannot be visually observed; that is, it happens so quickly that the global torque maximum is coincident with the local torque maximum due to feeding, and the first obtainable visual data point is too late to capture visual evidence of the phase inversion [23,26,27]. Scott and Joung, working with immiscible blends of similar absolute viscosity, did not observe the global torque maximum signifying phase inversion until approximately 3 min mixing time for a $\lambda = 0.05$ blend and approximately 10 min for a $\lambda = 0.003$ blend [23]. In this work, the $\lambda = 0.003$ miscible blend takes 84 s to achieve the global torque maximum, so based on the work by Scott and Joung, the comparable time-to-phase inversion for the $\lambda = 0.03$ blend should be approximately 25 s, making the torque global maximum and feeding peaks coincident and indistinguishable. Additionally, this transition occurs before the first sampling point at 30 s mixing time, thus subverting any visual evidence of the phase-inversion-like process. Using the mechanism proposed for phase inversion in immiscible blends proposed by Lazo [29], the enhanced rate of the phase-inversion-like process in miscible blends versus their immiscible counterparts is attributed to a decreased energetic penalty for sheet formation and spreading due to the decreased interfacial tension. (For a discussion of interfacial tension vis-à-vis miscible systems, please see Refs. [17,30].)

It is likewise worthwhile to mention that this phase-inversion-like process is not due to manipulating differences in transition temperature via a temperature-ramping protocol, as was shown by previous investigators for phase inversion in immiscible blends [31–34]; these materials all have essential the same transition temperature of approximately 100°C.

A second fundamental observation regarding mixing in low-viscosity, miscible blends is the deleterious effect the low-viscosity, minor-phase component has upon the rate of

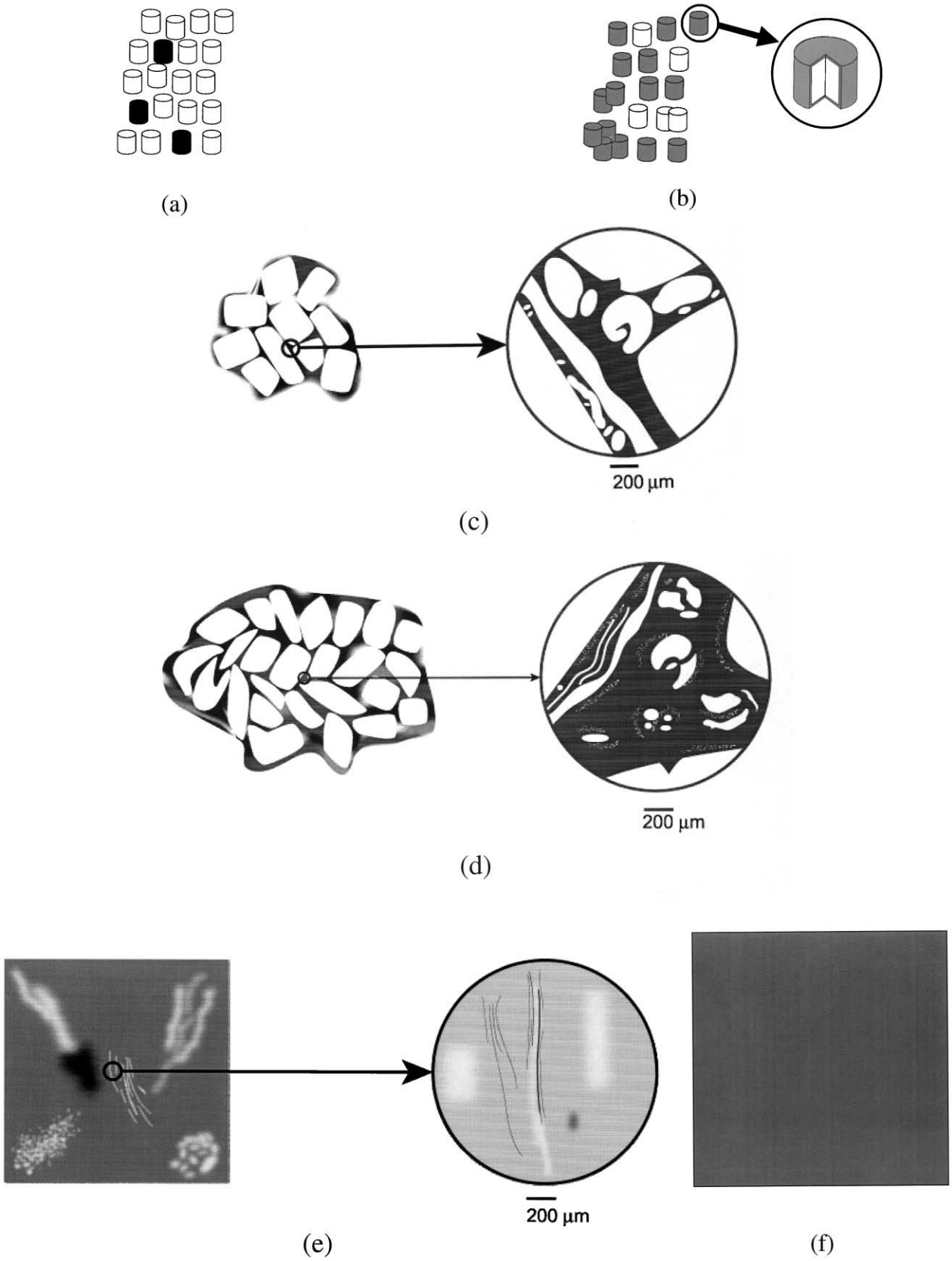

Fig. 11. Schematic representation of the morphological evolution as a function of mixing time in low-viscosity, miscible polymer blends.

mixing. As previously discussed, low-viscosity additives tend to migrate to high-shear-rate regions of the mixing equipment, where they act as lubricants and retard the mixing process. This work has shown that miscibility does not overcome this segregation tendency. Evidence of this is found in Fig. 1, the normalized mixing torque as a function of time and viscosity ratio. This figure shows the forward progression in time of the maximum mixing torque peak as viscosity ratio decreases; that is, the smaller the viscosity ratio, the longer it takes for the maximum mixing torque to be reached. As the maximum mixing torque has been shown to correspond to softening/melting of the high-viscosity, major-phase component [23], which is obligatory if the blend is to be thoroughly mixed, this necessarily delays the mixing process. Visual evidence of this delay can also be seen by comparing Figs. 3 and 4(b). Fig. 4(b), a low-magnification photograph of the $\lambda = 0.003$ blend at 46 s mixing time, shows significantly more undeformed pellets present than Fig. 3, which depicts the $\lambda = 0.03$ blend at 45 s mixing time. As in immiscible blends, this delay is due to the lubricative effects of the additive: it decreases both the amount of energy available to soften/melt the dispersed major phase by decreasing the viscous dissipation and the stress transfer to the major-phase pellets. Both of these effects are controlled by the additive's viscosity, so the lower the viscosity, the more pronounced is the delay in the mixing process. Once again, these low-viscosity-ratio, miscible polymer blends exhibit a dynamic similarity to their immiscible counterparts: the presence of the low-viscosity additive significantly delays the mixing process.

All of these experiments and observations of the morphological development in these low-viscosity-ratio, miscible polymer blends allow a both a time-line and a schematic representation of morphological change to be constructed. This schematic drawing is shown in Fig. 11. (For the purposes of this discussion, we will confine ourselves to the $\lambda = 0.003$ and $\lambda = 0.00015$ blends, in which this phase-inversion-like process occurs slowly enough so that most aspects of it may be visually observed and documented.) Initially, a salt-and-pepper mixture of pellets of the high-viscosity, major-phase material (white) and the low-viscosity, miscible minor-phase additive (black) are added to the batch mixer, as shown in Fig. 11(a). At the first sampling point, generally at the time of the local torque maximum due to feeding, the morphology consists of a granular mixture of solid, undeformed major-phase pellets, most of which are encapsulated by a thin layer of molten, minor phase material, as seen in Fig. 11(b). Some uncoated pellets remain, however, as illustrated by the white pellets in Fig. 11(b). There may be a few small clumps of a few pellets that are agglomerated, but the mixture is still largely free-flowing because the melt viscosity of the minor component is insufficient to act as an adhesive between the major-phase pellets.

At the next sampling point, generally taken at the local torque minimum after the feed maximum, the size of the pellet agglomerates has increased and the pellets themselves have begun slight macroscopic deformation. Additionally, some of the major-phase material has been sheared off the pellet cores, as predicted by the Scott/Macosko mechanism, generating a significant interstitial morphology of sheets, striations, and droplets observed in micrographs of blends. The characteristic size scales of this interstitial morphology are widely dispersed, ranging between 10 and 300 μm. This morphological state is depicted in Fig. 11(c).

The third sample, generally taken as the mixing torque approaches approximately one-third to one-half of its global maximum, is shown in Fig. 11(d). There is a continued increase in the size of the agglomerated pellet clumps; additionally, the pellets themselves exhibit an increase in their macroscopic deformation. Individual pellets and their boundaries are still distinguishable, however. There is likewise an increase in the amount of interstitial morphology, but a decrease in its overall characteristic size scale. More, finer droplets and sheets begin to appear as the larger droplets and sheets of the previous time step begin to break up.

By the time the fourth time sample is taken, generally at the global torque maximum, individual pellets are no longer distinguishable in the macroscopic sample. In fact, at some point between the third and fourth samples, the mixture abruptly consolidates and becomes fully molten, with a very limited number of regions of deformed but as-yet undispersed major-phase material. This is represented in Fig. 11(e). The attendant microscopic morphology appears largely homogeneous, with only a few very fine striations/sheets at a size scale of approximately 10 μm, and the rare region of major-phase material. It is at this point that the dynamic size scale problem inherent in all mixing studies becomes apparent: while some interesting events are still occurring on the macroscopic level, the interstitial morphology is too fine to resolve optically because of either its size or the nearly-uniform dispersion of the pigment particles used to provide the initial contrast. In the case of immiscible blends, this problem is easily resolved by selective extraction of one blend component, then interrogation of the resulting carcass using electron microscopy; this is not feasible with miscible blends because the nearly-equivalent solubility parameters of the miscible components prevent this selective extraction. Therefore, no smaller-size-scale morphologies can be ascertained for these miscible blends.

Finally, at long mixing times, (taken as 5 min in these experiments) the blend becomes completely homogeneous and assumes a single-phase, solid-solution morphology, as shown in Fig. 11(f).

The transition from a morphology of largely-undeformed pellets dispersed in a matrix of molten minor-phase material to that of a fully-consolidated, molten blend occurs very abruptly; in the case of the $\lambda = 0.003$ blend, the transition occurs between 46 and 60 s mixing. We hypothesize that this transition is controlled by the softening behavior of the major-phase pellets. That is, the blend becomes fully molten

and consolidates when the temperature of the major-phase pellets reaches a sufficient value that the material can flow readily. Modeling the major-phase pellets as spheres of equivalent radii with constant thermal properties and neglecting the attendant phase transition, it takes approximately 38 s for a pellet with the physical properties of the major-phase PE to reach the mixing temperature, 180°C, from the feed temperature, 25°C. This assumes a convective heat transfer boundary condition at the sphere's surface and a heat transfer coefficient of 600 J/m^2 s K. This heat transfer coefficient was derived from a correlation by Deopura and Scott [35]. If the phase transition were accounted for, and the time required to melt the minor-phase material needed to fulfill the heat-transfer boundary condition were added, then the time for the sphere to reach the mixing time at its center is certainly on the order of the observed time-to-consolidation, approximately 50 s.

Ratnagiri has postulated a model for predicting the time-to-phase-inversion in immiscible polymer systems based on a critical accumulated strain that must be reached before phase inversion can occur [27]. Using the Haake mixer and roller blades to compound an immiscible blend of polystyrene (PS) and PE having $\lambda = 0.003$, he found a critical accumulated strain of 22 was required to bring about phase inversion. In the corresponding miscible system, assuming a time-to-phase-inversion of 50 s, Ratnagiri's model predicts that the corresponding accumulated strain is only 2. We attribute this difference, once again, to the ease of sheet formation and film draining facilitated by the decreased interfacial tension in this miscible blend. It is important to understand that in Ratnagiri's work, and also that of Lazo [29], the accumulated strain is directly correlateable to the visualizable, quantifiable thinning of polymer sheets, which facilitates phase inversion. In these miscible blends, we see some accumulated strain vis-à-vis the increased deformation of the major-phase pellets, but we do not possess such detailed information because of the inability of the pigmentation contrast mechanism to elucidate these sheets and their dimensions.

5. Conclusions

In this work, the effect of viscosity ratio upon the mixing process in miscible polymer blends was investigated using model blends of SAN/PMMA and PE/PE. This work reconfirms the importance of the softening/melting regime to the development of morphology in miscible blends in general, and in low-viscosity-ratio miscible blends in particular. Additionally, these experiments have extended the previously-seen dynamic similarity between the short-mixing-time behavior of miscible blends and their immiscible counterparts to include even low-viscosity-ratio blends. The torque traces for very low viscosity ratio ($\lambda = 0.003$ and $\lambda = 0.00015$) blends exhibit both a local and a global maximum. Furthermore, photographs of short-mixing-time samples for these blends reveal a morphology of largely-undeformed major-phase pellets encapsulated by molten minor-phase material, while longer time samples are shown to be molten and consolidated. These are the first such observations for a miscible polymer blend and are compellingly reminiscent of the phase inversion process seen in low-viscosity-ratio immiscible polymer blends. This extends the dynamic similarity to include not only the importance of the softening/melting regime and the operation of the Scott/Macosko mechanism, but also the phase inversion process as well.

We postulate a macroscopic mechanism of morphology development in which the minor-phase component melts, encapsulating still-solid major-phase pellets. Some of the major-phase material undergoes the Scott/Macosko mechanism, rapidly generating a bimodal distribution of characteristic size scales, with largely-undeformed pellets coexisting alongside sheets, droplets, and striations. As mixing progresses in the softening/melting regime, the size of this interstitial morphology decreases. Eventually, when the major-phase pellets reach a sufficiently high temperature so the material can flow easily, the blend consolidates into a fully molten mass with little distinguishable morphology.

The presence of a very-low-viscosity, miscible component delays the onset of mixing, as evidenced by the shift in the maximum torque peak, as well as the presence of increased numbers of largely-undeformed pellets present at longer mixing times. This is due to the lubricating effect of the low-viscosity additive component, which reduces the stress transfer to the dispersed major-phase component and slows its deformation and breakup.

Acknowledgements

This work made use of MRSEC Shared Facilities supported by the National Science Foundation under Award Number DMR-9400334. The authors wish to acknowledge the National Science Foundation for support of H.E.B. with a Graduate Student Fellowship during the course of this work. Additional thanks are extended to Terry L. Virkler of the Bayer Corporation for providing the custom-synthesized, low-viscosity SANs. Karen E. Shafer was instrumental in the digital-image-capture microscopy.

References

[1] Grace HP. Chem Engng Comm 1982;14:225.
[2] Irving HF, Saxton RL. Mixing of high viscosity materials. In: Uhl VW, Gray JB, editors. Mixing theory and practice. New York: Academic Press, 1967. p. 169–224.
[3] Tadmor Z, Gogos CG. Principles of polymer processing. New York: Wiley, 1979.
[4] Khan MB, Briscoe BJ, Richardson SM. Polym-Plast Technol Engng 1994;33(3):295–322.
[5] MacLean DL. J Rheol 1973;17(3):385–99.

[6] Scott CE, Macosko CW. Polym Bull 1991;26:341–8.
[7] Sundararaj U, Macosko CW, Rolando RJ, Chan HT. Polym Engng Sci 1992;32(24):1814–23.
[8] Lindt JT, Ghosh AK. Polym Engng Sci 1992;32(24):1802–13.
[9] Spencer RS, Wiley RM. J Colloid Sci 1951;6:133–45.
[10] Erwin L. Polym Engng Sci 1978;18(13):1044–8.
[11] Ottino JM, Ranz WE, Macosko CW. Chem Engng Sci 1979;34:877–90.
[12] Ottino JM, Chella R. Polym Engng Sci 1983;23(7):357–79.
[13] Baim W, Bigio D. ANTEC 1994;40:266–9.
[14] Murakami Y, Fujimoto K, Uotani S. J Chem Engr Jpn 1972;5(1):85–6.
[15] Ng KY, Erwin L. Polym Engng Sci 1981;21(4):212–7.
[16] Scott CE, Macosko CW. Polymer 1995;36(3):461–70.
[17] Burch HE, Scott CE. Polym Engng Sci 2001 (in press).
[18] Paul DR, Barlow JW. J Macrmol Sci — Rev Macromol Chem 1980;C18(1):109–68.
[19] Hu S-R, Kyu T, Stein RS. J Polym Sci B 1987;25:71–87.
[20] Norton DR, Keller A. J Mat Sci 1984;19:447–56.
[21] Runt JP. Crystalline polymer blends. In: Paul DR, Bucknall CB, editors. Polymer blends volume 1: formulation. New York: Wiley, 2000. p. 167–86.
[22] Thomas EL, personal communication, 2000.
[23] Scott CE, Joung SK. Polym Engng Sci 1996;36(12):1666–74.
[24] Piglowski J, Kressler J, Kammer HW. Polym Bull 1986;16(6):493–7.
[25] Pearson DS, Ver Strate G, von Meerwall E, Schilling FC. Macromolecules 1987;20:1133–41.
[26] Ratnagiri R, Scott CE. Polym Engng Sci 1998;38(10):1751–62.
[27] Ratnagiri R, PhD Thesis, Massachusetts Institute of Technology, 2000.
[28] Sundararaj UT, PhD Thesis, University of Minnesota, 1994.
[29] Lazo NDB, PhD Thesis, Massachusetts Institute of Technology, 2000.
[30] Joseph DD. Eur J Mech, B/Fluids 1990;9(6):565–96.
[31] Shih C-K. Adv Polym Tech 1992;11(3):223.
[32] Shih C-K. Polym Engng Sci 1995;35(21):1688.
[33] Shih C-K, Tynan DG, Denelsbeck DA. Polym Engng Sci 1991;31(23):1670–3.
[34] Sundararaj UT, Macosko CW, Shih C-K. Polym Engng Sci 1996;36(13):1769.
[35] Deopura M, Scott CE. ANTEC 2000;46:418–22.